Check for updates

Geophysical Research Letters

RESEARCH LETTER
10.1029/2025GL115548

# Sub-Footprint Spatial Inhomogeneity Effect on Geostationary Hyperspectral Infrared Sounder Radiance Simulation

**Di Di[1,2], Pengyu Huang[3], Bo Li[4,5], Min Min[3], Zhenglong Li[6], W. Paul Menzel[6], Jun Li[4,5], and Myoung-Hwan Ahn[7]**

[1]Collaborative Innovation Center on Forecast and Evaluation of Meteorological Disasters, Nanjing University of Information Science and Technology, Nanjing, China, [2]Key Laboratory for Aerosol-Cloud-Precipitation of China Meteorological Administration, School of Atmospheric Physics, Nanjing University of Information Science and Technology, Nanjing, China, [3]School of Atmospheric Sciences and Guangdong Province Key Laboratory for Climate Change and Natural Disaster Studies, Sun Yat-Sen University and Southern Marine Science and Engineering Guangdong Laboratory (Zhuhai), Zhuhai, China, [4]Key Laboratory of Radiometric Calibration and Validation for Environmental Satellites, National Satellite Meteorological Center (National Center for Space Weather), Beijing, China, [5]Innovation Center for FengYun Meteorological Satellite, China Meteorological Administration, Beijing, China, [6]Cooperative Institute for Meteorological Satellite Studies, University of Wisconsin-Madison, Madison, WI, USA, [7]School of Engineering, Ewha Womans University, Seoul, Korea

**Key Points:**

- Sub-footprint atmospheric spatial inhomogeneity has a substantial effect on geostationary hyperspectral IR sounder brightness temperature simulation depending on the spatial resolution
- Spatial inhomogeneity effect is much larger over land than over ocean and influences more on lower tropospheric information extraction
- It is recommended that atmospheric spatial inhomogeneity effects should be considered in profile retrieval or data assimilation

**Correspondence to:**

J. Li and P. Huang,
junli@cma.gov.cn;
huangpy29@mail2.sysu.edu.cn

**Citation:**

Di, D., Huang, P., Li, B., Min, M., Li, Z., Menzel, W.P., et al. (2025). Sub-footprint spatial inhomogeneity effect on geostationary hyperspectral infrared sounder radiance simulation. *Geophysical Research Letters*, *52*, e2025GL115548. https://doi.org/10.1029/2025GL115548

Received 25 FEB 2025
Accepted 30 MAY 2025

**Author Contributions:**

**Conceptualization:** Di Di, W. Paul Menzel, Jun Li, Myoung-Hwan Ahn
**Formal analysis:** Bo Li
**Funding acquisition:** Jun Li
**Investigation:** Bo Li, Min Min, Zhenglong Li
**Methodology:** Di Di, Pengyu Huang
**Software:** Di Di, Pengyu Huang
**Supervision:** Jun Li
**Validation:** Min Min
**Visualization:** Di Di
**Writing – original draft:** Jun Li
**Writing – review & editing:** Bo Li, Min Min, Zhenglong Li, W. Paul Menzel, Myoung-Hwan Ahn

© 2025. The Author(s).
This is an open access article under the terms of the Creative Commons Attribution-NonCommercial-NoDerivs License, which permits use and distribution in any medium, provided the original work is properly cited, the use is non-commercial and no modifications or adaptations are made.

**Abstract** Hyperspectral infrared (IR) sounders onboard the geostationary satellites have revolutionized our understanding of Earth's atmosphere by providing detailed measurements of temperature, moisture, and trace gases with high temporal resolution. However, the accuracy of these measurements and corresponding simulations can be affected by the sub-footprint atmospheric spatial variations. In this study, we investigated the impact of sub-footprint atmospheric spatial inhomogeneity (SASI) effects on geostationary hyperspectral IR sounder (GeoHIS) radiance simulations with very high spatial resolution atmospheric profiles across different spectral channels and viewing geometries under clear-sky conditions. Results reveal significant deviations greater than 1.0 K between simulated radiances considering SASI effects and those assuming a plane-parallel atmosphere, especially for weak absorption and window channels. These deviations exhibit strong spectral and view angle dependencies, emphasizing the importance of accounting for SASI effects in representativeness error estimation, instrument inter-comparisons, sounding retrievals and data assimilation in numerical weather prediction using GeoHIS radiances.

**Plain Language Summary** Hyperspectral infrared sounders onboard the geostationary orbital satellites enable viewing the three-dimensional atmosphere frequently. China has such an instrument called Geostationary Interferometric Infrared Sounder onboard both Fengyun-4A and Fengyun-4B, Europe will have Infra-Red Sounder (IRS) onboard MTG in the 2025/2026-time frame, and U.S. is planning for the GeoXO sounder (GXS) in the next decade. Other countries like Japan, Korea, and India are also planning for geostationary hyperspectral IR sounder (GeoHIS) systems. IRS and GXS will have a spatial resolution of 4 km at nadir and a temporal resolution of 1 hr or better, helping scientists understand the Earth's atmosphere by monitoring changes of atmospheric temperature, moisture, and trace gases in detail. However, assuming that the atmosphere is homogeneous can lead to errors. Our study looks at how small, sub-footprint atmospheric variations (or so-called sub-footprint atmospheric spatial inhomogeneity [SASI] effects) can change the measurements that these instruments make. Using numerical simulations with high resolution data, we found that these SASI effects can make a significant difference in the measurements, especially when looking at temperature and moisture in the atmosphere. This means that scientists need to consider these SASI effects to get more accurate determinations of atmospheric temperature, moisture, and trace gases from these GeoHIS instruments.

## 1. Introduction

Hyperspectral infrared (IR) sounders onboard both polar orbiting and geostationary satellites have emerged as indispensable tools in atmospheric sciences, offering unparalleled capabilities to view Earth's atmosphere with high spectral resolution and wide spatial coverage. Most of these instruments, deployed aboard polar

19448007, 2025, 12, Downloaded from https://agupubs.onlinelibrary.wiley.com/doi/10.1029/2025GL115548 by Ewha Womans University Library, Wiley Online Library on [07/12/2025]. See the Terms and Conditions (https://onlinelibrary.wiley.com/terms-and-conditions) on Wiley Online Library for rules of use; OA articles are governed by the applicable Creative Commons License

orbiting satellite platforms, such as the Atmospheric Infrared Sounder, Cross-track Infrared Sounder, Infrared Atmospheric Sounding Interferometer (IASI), and Hyperspectral Infrared Atmospheric Sounder (Menzel et al., 2018), provide valuable measurements for a wide range of applications, including weather forecasting, climate monitoring, air quality assessment, and environmental research. The fundamental purpose underlying the operation of hyperspectral IR sounders lies in their ability to measure IR radiation emitted by the atmosphere across a broad spectral range. By analyzing the spectral characteristics of this radiation, essential atmospheric parameters such as temperature, humidity, cloud properties, and trace gas concentrations can be retrieved. These radiance measurements and the derived atmospheric parameters play a crucial role in improving our understanding of atmospheric dynamics, energy budget, and composition, thus facilitating advancements in weather prediction accuracy, climate modeling fidelity, and environmental management strategies.

Recently, the hyperspectral IR sounders onboard the geostationary weather satellites introduced another advancement in sounding the atmosphere from space. The Geostationary Interferometric Infrared Sounder (GIIRS) onboard the Fengyun-4A became the first geostationary hyperspectral IR sounder (GeoHIS) and was followed by another GIIRS onboard Fengyun-4B. Europe will operate a GeoHIS (Holmlund et al., 2021) called Infra-Red Sounder (IRS) onboard Metoesat Third Generation-Sounder; U.S. and Japan are also planning future GeoHIS (Bessho et al., 2025) onboard their next generation of geostationary observing systems (Lindsey et al., 2024). Measurements from GeoHIS provide detailed information frequently of a weather cube, and can detail fast-changing atmospheric structures; this adds unique value for nowcasting, monitoring and predicting the atmospheric environment, etc. (J. Li, Menzel, et al., 2022). For example, GeoHIS measurements not only provide thermodynamic information for situation awareness through inversion of radiances to profiles of temperature and moisture (J. Li et al., 2024) but also improve numerical weather prediction (NWP) through direct assimilation of radiances (Yin et al., 2021). In addition, targeted GeoHIS measurements over a selected region with higher temporal resolution (Han et al., 2025) provide dynamic information (three dimensional horizontal winds) (J. Li, Zhang, et al., 2022; J. Li et al., 2025; Ma, Li, Han, et al., 2021) through tracking of moisture features. These 3D winds can provide added value on NWP-based high impact weather forecasts when assimilated together with other satellite measurements (Meng et al., 2024; Wang et al., 2025). However, the accuracy of atmospheric retrievals from GeoHIS hinges on the fidelity of radiative transfer simulations, which models the propagation of IR radiation through the atmosphere from the Earth's surface to the top of atmosphere. Traditionally, radiative transfer simulations have relied on simplified assumptions, such as a plane-parallel and horizontally homogeneous atmosphere within the satellite sounder's footprint. While these assumptions are reasonable for many applications, they fail to capture the intricate 3D structure of the atmosphere at smaller spatial scales, known as the sub-footprint atmospheric spatial inhomogeneity (SASI) effects, especially when the footprint size is large (Di et al., 2021).

At the sub-footprint level, the atmosphere exhibits significant spatial variability in temperature, humidity, and trace gas distributions, driven by a myriad of factors including terrain features, land surface properties, cloud morphology, and localized atmospheric phenomena. These SASI effects can exert a pronounced influence on the observed radiance spectra, introducing biases and uncertainties in the retrieved atmospheric parameters. Despite their potential impact, SASI effects have received limited attention in the context of hyperspectral IR sounder data interpretation. Although Di et al. (2021) has utilized the high spatial resolution Advanced Himawari Imager (AHI) to explore the sounder sub-footprint radiance inhomogeneity, there are three limitations on their study: (a) the spatial resolution of 2 km for AHI is not ideal for simulating sounders such as InfraRed Sounder (IRS) with high spatial resolution of 4 km at nadir, (b) AHI is a broad band imager, it cannot well represent the high spectral resolution sounder information, and (c) AHI has only limited number of absorption channels (three $H_2O$ and one $CO_2$ absorption channels). Therefore, lack of understanding the SASI effects still poses challenges to the accuracy and reliability of atmospheric retrievals.

In this paper, we address this critical gap in knowledge by investigating the SASI effect on GeoHIS radiance simulations, with special attention on those footprints with large viewing angles. The reason we chose GeoHIS instead of polar orbit sounders is that the zenith angle for geostationary sounder could be large than 60° (typical maximum for polar orbiters), and a large zenith angle results in coarse spatial resolution. Our study aims to comprehensively analyze how SASI effects and terrain features within the sounder's field-of-view (FOV or footprint) perturb the observed radiance spectra, leading to deviations from the traditional plane-parallel assumption. By leveraging advanced radiative transfer models and high-resolution atmospheric data sets, the

19448007, 2025, 12, Downloaded from https://agupubs.onlinelibrary.wiley.com/doi/10.1029/2025GL115548 by Ewha Womans University Library, Wiley Online Library on [07/12/2025]. See the Terms and Conditions (https://onlinelibrary.wiley.com/terms-and-conditions) on Wiley Online Library for rules of use; OA articles are governed by the applicable Creative Commons License

magnitude and spatial distribution of SASI effects across different spectral channels and viewing geometries are quantified. Furthermore, the implications of these effects for atmospheric retrievals are explored, their significance for improving the accuracy and robustness of hyperspectral infrared sounder products, as well as enhancing the data assimilation for NWP, are discussed.

## 2. Data and Methodology

### 2.1. Data

To investigate the impact of spatial response on simulated observations from a geostationary infrared hyperspectral instrument, this study uses ECMWF IFS Experimental Nature Run at 1-km (XNR1K) data with a spatial resolution of 1 km as the input for the simulation model (Wedi et al., 2020). The data used includes surface temperature, surface pressure, atmospheric temperature profile, and atmospheric humidity profile. There are 137 pressure layers in the vertical dimension, ranging from 0.02 to 1,012 hPa (ECMWF, 2024).

The radiative transfer model used in this study is RTTOV (version 13) (Hocking et al., 2021), combined with the FY-4B/GIIRS coefficient files provided on the official website to ensure that the simulated spectral characteristics align with the observed spectra from FY-4B/GIIRS. Please note that for the simulations in RTTOV, only the spatiotemporal variability in surface temperature, pressure, atmospheric temperature, and humidity profile are accounted for. Other trace gas profiles including ozone are fixed, following the 1976 US Standard Atmospheric profile or default reference profile in the RTTOV. FY-4B/GIIRS is an IR hyperspectral interferometer with two spectral bands: the long-wave band (680–1,130 $cm^{-1}$ or 8.85–14.71 μm) and the middle-wave band (1,650–2,250 $cm^{-1}$, or 4.44–6.06 μm), both with a spectral resolution of 0.625 $cm^{-1}$. In this study, it is assumed that the geostationary satellite with a hyperspectral IR sounder is located at longitude 104.7° (the FY-4A position) and the latitude-longitude lookup table for FY-4A/AGRI, provided by FENGYUN Satellite Data Center (FENGYUN Satellite Data Center, 2013), is used to ensure consistent simulation conditions. Four different nadir spatial resolutions (4, 8, 12, or 16 km at nadir) for the geostationary IR hyperspectral instruments are considered. These resolutions represent those from IRS, future GIIRS, GIIRS/FY-4B, and GIIRS/FY-4A, respectively. The FY-4A/AGRI lookup table corresponds to a 4 km resolution at nadir, with other resolutions determined through interpolation.

### 2.2. Methodologies

To simulate GeoHIS brightness temperatures (BTs) at different resolutions, the Point Spread Function (PSF) is applied to high resolution BTs with 1 km resolution. The PSF describes the response of a sensor to signals from different spatial locations. In this study, the PSF (Z. Li et al., 2023) used considers both the spatial resolution of the instrument at the target location and the central frequency of the detection channels. For example, the spatial resolution of 4 km at nadir (as shown in Figure 2b) increases with the satellite's zenith angle (doubling at approximately 65°). Since the PSF is channel dependent, it is calculated using the mean value approach (as shown in Equation 1) for this study, here, $r$ represents the spatial resolution at the target location, $wv$ is the central wavenumber of the current channel (in $cm^{-1}$), and $n$ denotes the total number of channels.

$$\mathrm{PSF}_r = \frac{1}{n}\sum \mathrm{PSF}_{r,wv} \tag{1}$$

This study quantifies the impact of sounder sub-footprint surface and atmospheric inhomogeneity and its influence on radiance simulation. The standard deviation (STD) of a variable ($X$) is calculated within a sub-footprint using Equation 2 for quantifying SASI effects, where $X_s$ denotes the variable mean value that accounts for spatial response, representing the radiance observation for the real situation. $M$ represents the number of samples with 1 km resolution found within a circle centered at the target's spatial location with a radius equal to half of the spatial resolution, and $i$ is the sample index within the circle.

When $X$ represents surface temperature ($T_{\mathrm{skin}}$), surface pressure (sp), temperature ($T$), or humidity ($Q$), the spatial response function for calculating $X_s$ is given by $\mathrm{PSF}_r$ (Equation 3).

$$\mathrm{STD}(X) = \frac{1}{M}\sum_{i=1}^{M}(X_s - X_i)^2 \tag{2}$$

$$X_s = \frac{1}{M}\sum_{i=1}^{M}\mathrm{PSF}_r(X_i),\ X = T_{\mathrm{skin}}, \mathrm{sp}, T, Q \tag{3}$$

This study explores the impact of SASI effect by discussing the characteristics in BT STD (Equations 4 and 5). In calculating $\mathrm{BT}_{\mathrm{SASI}}$, we first compute Rad (radiance) using Equation 5 and then convert Rad into BT using Planck's law.

$$\mathrm{STD}(\mathrm{BT}) = \frac{1}{M}\sum_{i=1}^{M}(\mathrm{BT}_{\mathrm{SASI}} - \mathrm{BT}_i)^2 \tag{4}$$

$$\mathrm{Rad} = \frac{1}{M}\sum_{i=1}^{M}\mathrm{PSF}_{r,wv}(\mathrm{Rad}_i) \tag{5}$$

$$\mathrm{BT}_{\mathrm{SASI}} = \mathrm{Plack}(\mathrm{Rad}) \tag{6}$$

The BT STD is used to quantify the magnitude of SASI effect caused by sub-footprint inhomogeneity. The STD is calculated based on samples within the 2nd to 98th percentile range to minimize the influence of extreme outliers. The larger the BT STD, the bigger the SASI effect. Due to the large number of channels in the GIIRS instrument, it is not feasible to present results for all channels in this study. Therefore, seven representative channels have been selected for discussion. Figure 1 shows the spectral positions of these channels, specifically including: the upper-level temperature channel (705 $\mathrm{cm}^{-1}$), mid-level temperature channel (714.375 $\mathrm{cm}^{-1}$), lower-level temperature channel (750.625 $\mathrm{cm}^{-1}$) in $CO_2$ absorption spectral region, upper-level humidity channel (1,663.75 $\mathrm{cm}^{-1}$), mid-level humidity channel (1,813.75 $\mathrm{cm}^{-1}$), lower-level humidity channel (1,978.75 $\mathrm{cm}^{-1}$) in $H_2O$ absorption spectral region, and the surface channel (909.375 $\mathrm{cm}^{-1}$) in window spectral region. Additionally, Figure 1 also displays the Jacobian functions calculated based on the 1976 U.S. Standard Atmosphere Profile, for the three temperature channels (temperature Jacobians) and three humidity channels (water vapor Jacobians).

## 3. Results and Analysis

The SASI effects can be obtained via the STD analysis with simulation, which allows us to quantify the deviations caused by sub-footprint inhomogeneity and assess their impact on radiance observations.

### 3.1. Sub-Footprint Atmospheric Spatial Inhomogeneity

The SASI effect results from the sub-footprint inhomogeneity. Figure 2a shows the distribution of BT in the 11 μm channel (909.375 $\mathrm{cm}^{-1}$) at a spatial resolution of 4 km at nadir. Note that the spatial resolution varies with viewing angle as shown in Figure 2b with a spatial resolution of 4 km at nadir. Figures 2e–2h shows the STD of surface temperature, surface pressure, 500 hPa temperature, 500 hPa humidity, 850 hPa temperature, and 850 hPa humidity, respectively.

The results in Figure 2 confirm and quantify the expected stronger sub-footprint inhomogeneity in the lower atmosphere (e.g., 850 hPa) compared to the mid-troposphere (e.g., 500 hPa). Surface skin temperature and surface pressure have more sub-footprint inhomogeneity, indicating the difficulty in retrieving boundary layer temperature and moisture profiles since all channels sensitive to the boundary atmosphere are also influenced by surface skin temperature and pressure. Hyperspectral IR sounder data alone might not be adequate to retrieval lower-level atmospheric profiles with high accuracy. Combination with surface station measurements could partially improve the lower-level atmospheric profile either through physical adjustments (Deng et al., 2024), or through joint variational methods (Zhou et al., 2025).



19448007, 2025, 12, Downloaded from https://agupubs.onlinelibrary.wiley.com/doi/10.1029/2025GL115548 by Ewha Womans University Library, Wiley Online Library on [07/12/2025]. See the Terms and Conditions (https://onlinelibrary.wiley.com/terms-and-conditions) on Wiley Online Library for rules of use; OA articles are governed by the applicable Creative Commons License

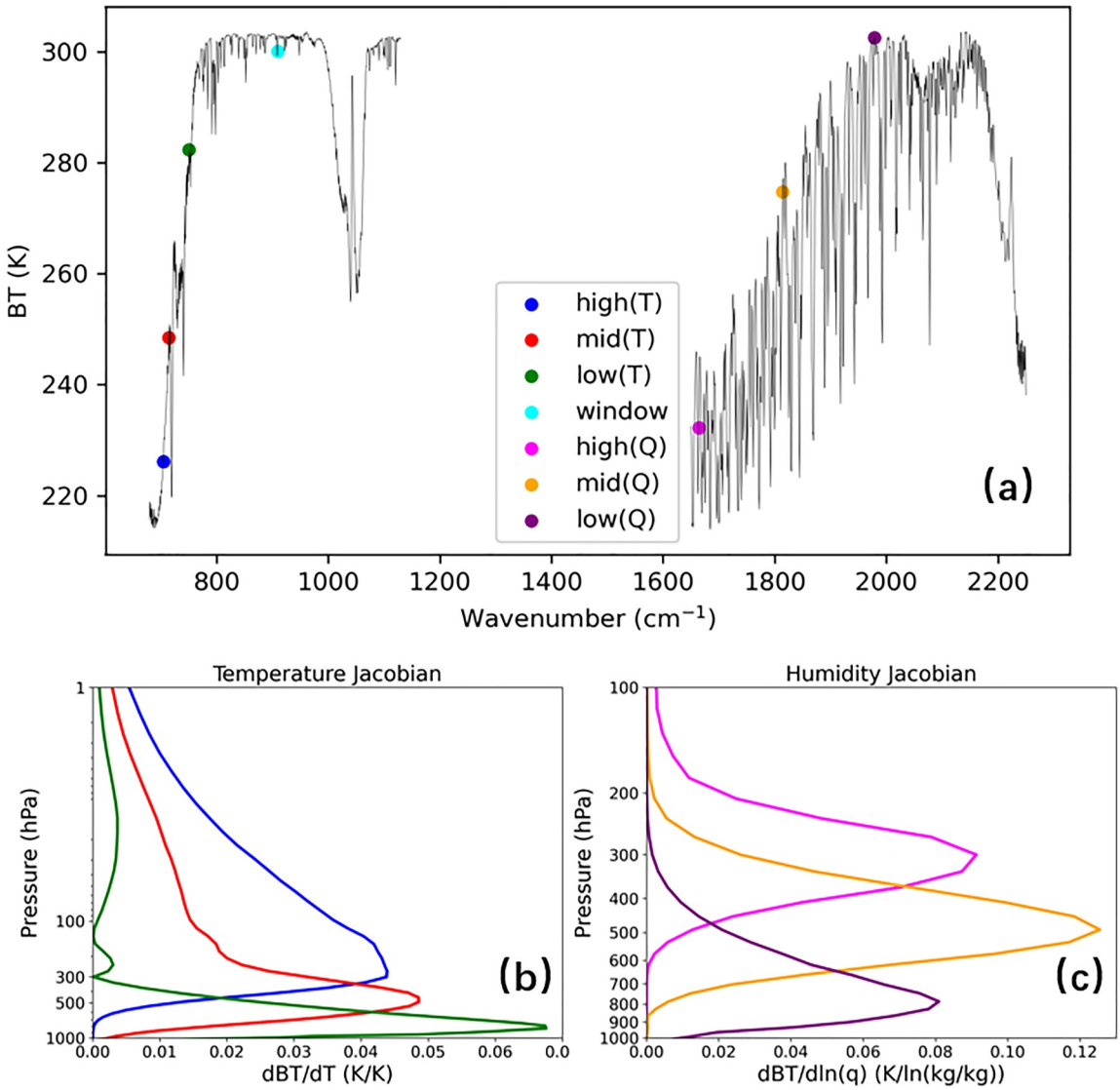



**Figure 1.** (a) The spectral positions of the target channels for this experiment and plots of the Jacobian functions for (b) three temperature channels and (c) three humidity channels. The legend displays the colors corresponding to different target channels, where "high," "mid," "low," and "window" represent the upper, middle, lower layers, and the window region, respectively. "T" and "Q" represent temperature and humidity, respectively.

### 3.2. Spectral Characteristics of SASI Effects

One important question is how the sub-footprint inhomogeneity influences the radiances with respect to different spectral regions and zenith angles. Figures 3a–3d show the sub-footprint BT STD spectra at spatial resolutions of 4, 8, 12, and 16 km at nadir, respectively. Each panel includes six lines: the blue, red, and green curves represent the BT STD for land with zenith angles of 0°–30°, 30°–45°, and 45°–67°, respectively; the pink, yellow, and purple curves represent the BT STD for ocean with zenith angles of 0°–30°, 30°–45°, and 45°–67°, respectively. The horizontal coordinate represents the center wavenumber of each channel, and the vertical coordinate represents the BT STD. The results reveal the following facts:

- The window spectral region (750–1,150 cm$^{-1}$ minus the ozone absorption band) and the shortwave IR region (1,950–2,250 cm$^{-1}$) have larger sub-footprint BT STD than the $CO_2$, $O_3$, and $H_2O$ absorption regions. This is consistent with the fact that surface and lower-level atmosphere have larger sub-footprint inhomogeneity (Figure 2). The sub-footprint BT STD could reach 0.5, 0.7, 0.9, and 1.1 K for the spatial resolution of 4, 8, 12,



19448007, 2025, 12, Downloaded from https://agupubs.onlinelibrary.wiley.com/doi/10.1029/2025GL115548 by Ewha Womans University Library, Wiley Online Library on [07/12/2025]. See the Terms and Conditions (https://onlinelibrary.wiley.com/terms-and-conditions) on Wiley Online Library for rules of use; OA articles are governed by the applicable Creative Commons License

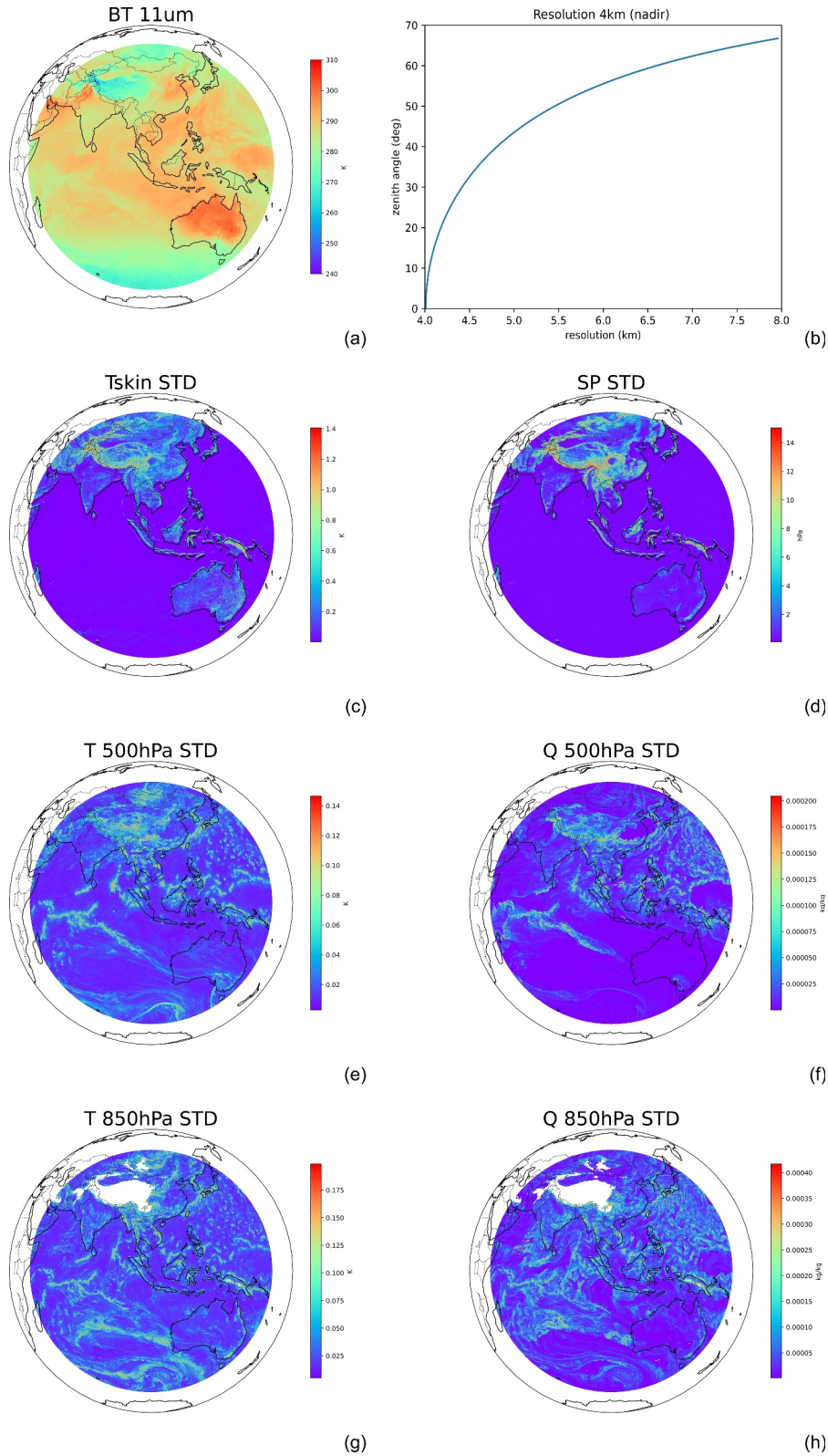



**Figure 2.** (a) The distribution of brightness temperature in the 11 μm channel (909.375 $cm^{-1}$) at a spatial resolution of 4 km. (b) The variation of the spatial resolution of the observed target with the zenith angle, at a spatial resolution of 4 km at nadir. (c–h) The standard deviation of surface temperature, surface pressure, 500 hPa temperature, 500 hPa humidity, 850 hPa temperature, and 850 hPa humidity, respectively (data corresponding to 00:15 UTC on 6 September 2019).



19448007, 2025, 12, Downloaded from https://agupubs.onlinelibrary.wiley.com/doi/10.1029/2025GL115548 by Ewha Womans University Library, Wiley Online Library on [07/12/2025]. See the Terms and Conditions (https://onlinelibrary.wiley.com/terms-and-conditions) on Wiley Online Library for rules of use; OA articles are governed by the applicable Creative Commons License

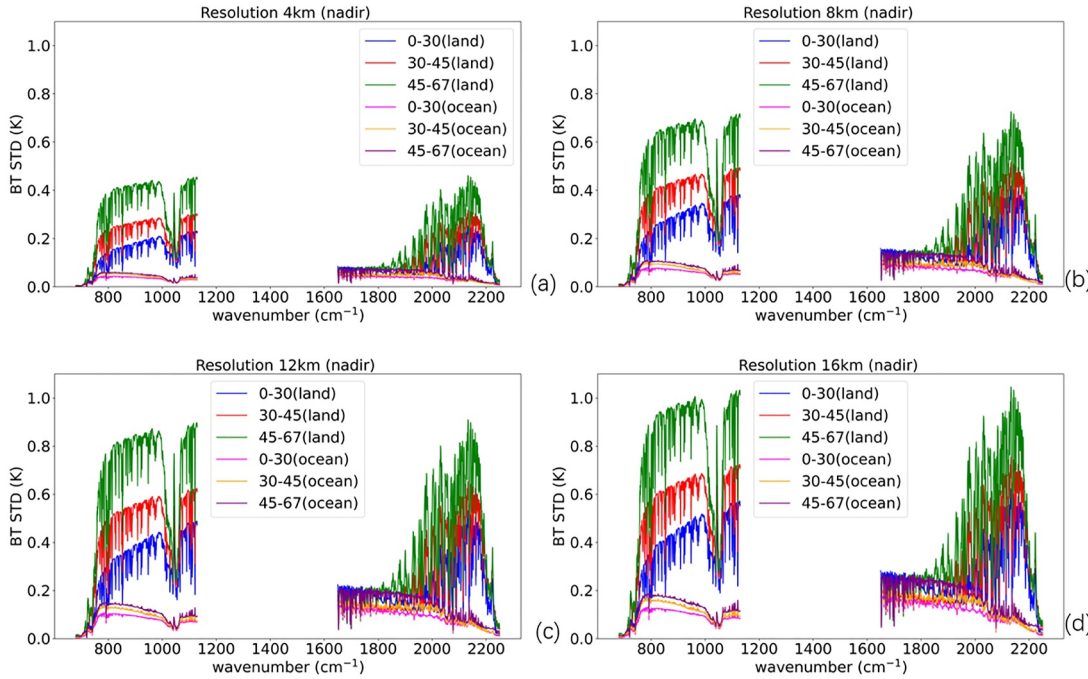



**Figure 3.** The sub-footprint brightness temperature (BT) standard deviation (STD) spectra at spatial resolutions of (a) 4, (b) 8, (c) 12, and (d) 16 km at nadir, respectively. Each figure includes six curves: the blue, red, and green curves represent the BT STD for land with zenith angles of 0°–30°, 30°–45°, and 45°–67°, respectively; the pink, yellow, and purple curves represent the BT STD for ocean with zenith angles of 0°–30°, 30°–45°, and 45°–67°, respectively. The horizontal coordinate represents the center wavenumber of each channel, and the vertical coordinate represents the BT STD.

and 16 km at nadir, respectively, over land at large zenith angles. STD values show a positive correlation with spatial resolution, particularly pronounced for window channels.

- Larger zenith angle results in larger sub-footprint BT STD. This is due the fact that larger footprint size has larger sub-footprint inhomogeneity. The impact of angle on sub-footprint BT STD is more in the window spectral region over land than over ocean, whereas the impact is smaller in the absorption spectral regions.
- SASI effect is much larger over land than over ocean, especially for lower-level (weak absorption) and window channels. Using a sounder with 4 km resolution at nadir as an example, the SASI effect can be 0.2–0.5 K depending on the zenith angle over land at the window spectral regions, while it is less than 0.1 K over ocean and less dependent on the zenith angle.

### 3.3. Spatial Characteristics of SASI Effects

Figure 4 shows the sub-footprint BT STD for the selected channels at a spatial resolution of 4 km at the nadir: (Figure 4a) the upper-level temperature channel (705 cm$^{-1}$), (Figure 4b) mid-level temperature channel (714.375 cm$^{-1}$), (Figure 4c) lower-level temperature channel (750.625 cm$^{-1}$), (Figure 4d) window region (909.375 cm$^{-1}$), (Figure 4e) upper-level humidity channel (1,663.75 cm$^{-1}$), (Figure 4f) mid-level humidity channel (1,813.75 cm$^{-1}$), and (Figure 4g) lower-level humidity channel (1,978.75 cm$^{-1}$), along with the (Figure 4h) mean BT STD for all channels. It can be seen that BT STD for the upper-level temperature channel (705 cm$^{-1}$) and mid-level temperature channel (714.375 cm$^{-1}$) are very small overall (less than 0.1 K), while the sub-footprint BT STD of lower-level temperature channel (750.625 cm$^{-1}$) is substantially larger than the high and middle-level temperature channels, reaching 0.4 K over land, especially over high terrains like Tibet Plateau (TP). The sub-footprint BT STD upper-level and middle-level humidity channels (1,663.75 and 1,813.75 cm$^{-1}$) is less affected by land surface since those channels contains less surface contribution, and it is usually less than 0.2 K. For the lower-level moisture channel (1,978.75 cm$^{-1}$), the sub-footprint BT STD is significantly larger than the middle and upper level channels since the radiance of the lower level moisture channel contain surface contributions, reaching 1.5 K over land, especially over high terrain such as the TP. Similar to the lower-level moisture channel, the window channel sub-footprint BT STD is significantly larger than the middle and upper level absorption channels. It is mainly affected by the land surface, especially by high terrain such as the TP. Therefore,



19448007, 2025, 12, Downloaded from https://agupubs.onlinelibrary.wiley.com/doi/10.1029/2025GL115548 by Ewha Womans University Library, Wiley Online Library on [07/12/2025]. See the Terms and Conditions (https://onlinelibrary.wiley.com/terms-and-conditions) on Wiley Online Library for rules of use; OA articles are governed by the applicable Creative Commons License

10.1029/2025GL115548

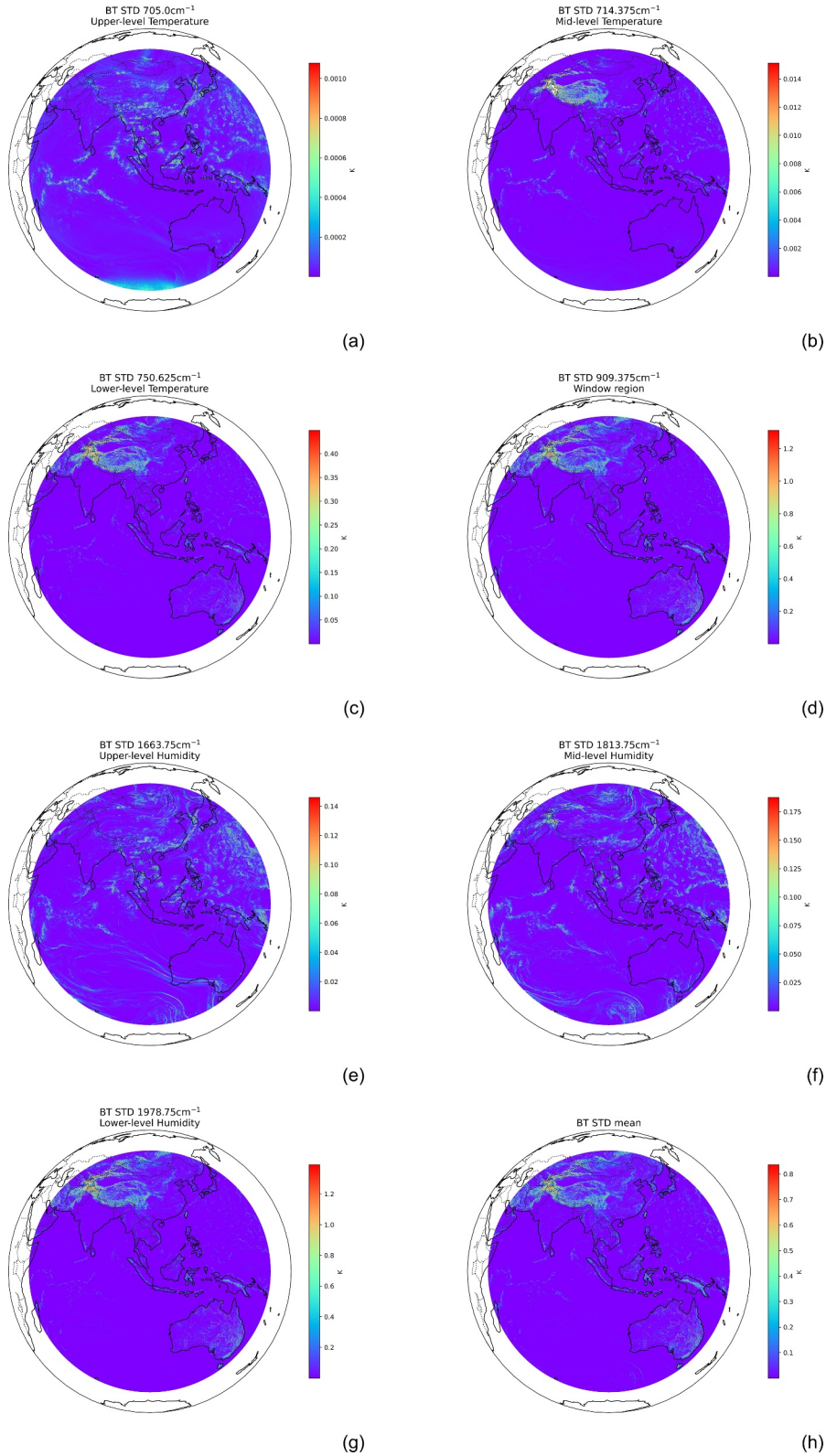



**Figure 4.** The sub-footprint brightness temperature (BT) standard deviation (STD) for the selected channels at a spatial resolution of 4 km at the nadir: (a) the upper-level temperature channel (705 $cm^{-1}$), (b) mid-level temperature channel (714.375 $cm^{-1}$), (c) lower-level temperature channel (750.625 $cm^{-1}$), (d) window region (909.375 $cm^{-1}$), (e) upper-level humidity channel (1,663.75 $cm^{-1}$), (f) mid-level humidity channel (1,813.75 $cm^{-1}$), and (g) lower-level humidity channel (1,978.75 $cm^{-1}$), along with the (h) mean BT STD for all channels.



19448007, 2025, 12, Downloaded from https://agupubs.onlinelibrary.wiley.com/doi/10.1029/2025GL115548 by Ewha Womans University Library, Wiley Online Library on [07/12/2025]. See the Terms and Conditions (https://onlinelibrary.wiley.com/terms-and-conditions) on Wiley Online Library for rules of use; OA articles are governed by the applicable Creative Commons License

19448007, 2025, 12, Downloaded from https://agupubs.onlinelibrary.wiley.com/doi/10.1029/2025GL115548 by Ewha Womans University Library, Wiley Online Library on [07/12/2025]. See the Terms and Conditions (https://onlinelibrary.wiley.com/terms-and-conditions) on Wiley Online Library for rules of use; OA articles are governed by the applicable Creative Commons License

the SASI effects for middle and upper temperature and moisture channels are usually less than 0.2 K and are less affected by surface contributions; lower-level channels, especially lower-level moisture channels and the window channels, have a significantly larger SASI effect, and the sub-footprint BT STD can reach 1.5 K over land, especially over high terrain regions.

## 4. Summary and Discussion

In this study, we investigated the impact of SASI effects on radiance simulations for hyperspectral IR sounders, to improve our understanding of atmospheric measurements from these instruments. Hyperspectral IR sounders play a crucial role in atmospheric sciences by providing detailed data on temperature, moisture, and trace gases. However, traditional simulations often assume a plane-parallel atmosphere, neglecting the spatial variability of atmospheric properties at smaller scales. Using 1 km spatial resolution profiles for simulating the GeoHIS with various spatial resolutions at nadir, the following has been found.

- Middle and upper tropospheric temperature and moisture show less SASI effects; usually the sub-footprint BT STD is less than 0.2 K. However, the lower tropospheric temperature and moisture channels along with the window channels show much larger SASI effects that are caused by sub-footprint inhomogeneities for lower-level atmosphere and surface (temperature and pressure); the sub-footprint BT STD could be greater than 1.0 K over land, mainly over the high terrain regions such as the TP.
- Higher spatial resolution shows less evidence of SASI effects; for example, when the spatial resolution is improved from 8 to 4 km at nadir, the SASI effect is reduced by 0.2 K for weak absorption and window channels.
- SASI effects are much larger over land than over ocean. In general, the SASI effect is less than 0.2 K over ocean for all channels, which has less impact on quantitative application such as sounding retrieval and data assimilation.

Through extensive numerical experiments and analysis, we demonstrated that nearby objects and terrain features can significantly influence the observed radiance spectra, deviating from the assumptions of a plane-parallel atmosphere. These SASI effects manifest as spectral variations and spatial gradients in the simulated radiances, impacting the accuracy and reliability of atmospheric retrievals and data assimilation. Our findings underscore the importance of considering SASI effects in radiance simulations for hyperspectral IR sounders to enhance the fidelity of atmospheric measurements.

Moving forward, it is essential to integrate these findings into the development of retrieval algorithms and data assimilation techniques for hyperspectral IR sounder data. By accounting for SASI effects, especially for those weak absorption and window channels over land, we can improve the accuracy and robustness of atmospheric retrievals. For example, observation errors for a typical sounders (e.g., IASI) are around 0.2–0.3 K accounting for radiometric and spectral calibrations, navigation, co-registration, and detector noise altogether for most tropospheric channels for a nominal atmosphere, if the sub-footprint homogeneity is greater than 0.5 K, the radiance for this FOV could be removed through quality control process. Or in term of retrieval accuracy requirement, if 1.5 K (temperature) and 15% (moisture) accuracy is required for profile retrievals, certain footprints with large sub-footprint homogeneity should be excluded in the processing or should be processed with additional information. For physical retrieval and data assimilation systems, the angle- and resolution-dependent SASI effects should be incorporated through dynamic adjustment of observation error covariance matrices to optimize channel weighting, particularly for homogeneous window channels over land. Other approaches include combining traditional 1Dvar and machine learning (Zhou et al., 2025) for removing surface contributions in radiance observations, incorporating ground station 2 m temperature and moisture information for improving the lower-level temperature and moisture profile retrieval either through physical method (Deng et al., 2024) or machine learning techniques (Ma, Li, Li, et al., 2021). Those channels affected by SASI effects should include those effects for data assimilation, especially over high terrains such as near the TP, currently, the assimilation of those surface/near-surface channels is limited partly due to the SASI effect, channel specific error covariance accounting for such effect could be beneficial for the variational type data utilization. It is worth noting that our estimation on SASI effect might be underestimated since we are using 1 km NWP data, which might underrepresent the real sub-footprint inhomogeneity. The slant path atmosphere (from satellite to ground) is not considered in this simulation, when the viewing angle is greater than 50°, vertical atmosphere assumption could bring additional uncertainty in BT simulation (Huang et al., 2024). Atmospheric profiles with spatial resolution higher than 1 km should

be better for quantifying the SASI effect for various applications. Another note is that only clear skies are assumed in our simulation study, which mainly reflects the sub-footprint surface and atmospheric inhomogeneity and its impact on radiance simulation. It is worthwhile to have further investigations in cloudy skies that might have different SASI effects associated with retrieval of cloud physical and optical properties. As noted, spatial variabilities of the surface and atmosphere contribute to the SASI effect, though their contributions vary across the spectrum. From Figures 2 and 4, we roughly infer that window channels (e.g., 909 $cm^{-1}$) show dominant surface influence (70%–80% of STD), evidenced by their strong correlation with skin temperature variability in Figure 2c. For lower-level channels like 750 $cm^{-1}$, surface contributions decrease to 40%–60%, while mid/upper-level channels are dominated by atmospheric signatures. This inference, however, is not entirely accurate. To quantify this more accurately, incorporating surface-atmosphere decoupling into our SASI effect research series is warranted. Specifically, replacing the model surface with a homogenous one could help us determine the proportion of variability arising from the surface versus the atmosphere as well as its spectral dependency. Beyond the SASI effect, the effect of temporal inhomogeneity—part of representation error stemming from the time difference between NWP and observations—caused by temporal variations in surface and atmospheric parameters is equally critical. Relevant quantitative research will be conducted for the AHI.

## Data Availability Statement

The data used in this study are available at Huang (2025). The version 13.2 of RTTOV (Saunders et al., 2018) used for radiance simulation is available at https://nwp-saf.eumetsat.int/site/software/rttov/.

**Acknowledgments**
This research is supported by the National Natural Science Foundation of China under Grants U2342201. We also used resources of the Oak Ridge Leadership Computing Facility at the Oak Ridge National Laboratory, which is supported by the Office of Science of the U.S. Department of Energy under Contract DE-AC05-00OR22725. We highly appreciate the valuable and insightful suggestions for future work from the anonymous reviewers.

## References

Bessho, K., Sakashita, T., Sumida, Y., Andou, A., Abe, M., Watanabe, I., et al. (2025). Status of Himawari-8/9 and their follow-on satellite Himawari-10. In *105th AMS annual meeting*. AMS.

Deng, C., Di, D., & Li, J. (2024). The effect of surface observations on enhancing the GIIRS thermodynamic profile retrieval. *Remote Sensing*, *16*(24), 4634. https://doi.org/10.3390/rs16244634

Di, D., Li, J., Li, Z., Li, J., Schmit, T. J., & Menzel, W. P. (2021). Can current hyperspectral infrared sounders capture the small scale atmospheric water vapor spatial variations? *Geophysical Research Letters*, *48*(21), e2021GL095825. https://doi.org/10.1029/2021gl095825

ECMWF. (2024). L137 model level definitions. Retrieved from https://confluence.ecmwf.int/display/UDOC/L137+model+level+definitions

FENGYUN Satellite Data Center. (2013). FY-4A AGRI [Dataset]. Retrieved from http://www.nsmc.org.cn/nsmc/cn/instrument/AGRI.html

Han, W., Yin, R., Li, J., Liu, Y., Wang, J., Li, Y., et al. (2025). Targeted sounding observations from geostationary satellite and impacts on high impact weather forecasts. *Science China Earth Sciences*, *68*(4), 963–976. https://doi.org/10.1007/s11430-024-1489-5

Hocking, J., Vidot, J., Brunel, P., Roquet, P., Silveira, B., Turner, E., & Lupu, C. (2021). A new gas absorption optical depth parameterisation for RTTOV version 13. *Geoscientific Model Development*, *14*(5), 2899–2915. https://doi.org/10.5194/gmd-14-2899-2021

Holmlund, K., Grandell, J., Schmetz, J., Stuhlmann, R., Bojkov, B., Munro, R., et al. (2021). Meteosat Third Generation (MTG): Continuation and innovation of observations from geostationary orbit. *Bulletin of the American Meteorological Society*, *102*(5), E990–E1015. https://doi.org/10.1175/bams-d-19-0304.1

Huang, P. (2025). Data and figures of "Sub-footprint atmospheric spatial inhomogeneity effect on geostationary hyperspectral infrared sounder radiance simulation" (version 1) [Dataset]. *figshare*. https://doi.org/10.6084/m9.figshare.28368629.v1

Huang, P., Li, J., Min, M., Li, Z., Di, D., Anantharaj, V., & Ahn, M.-H. (2024). Influence of atmospheric slant path on geostationary hyperspectral infrared sounder radiance simulations. *Geophysical Research Letters*, *51*(23), e2024GL110579. https://doi.org/10.1029/2024GL110579

Li, J., Menzel, W. P., Schmit, T. J., & Schmetz, J. (2022). Applications of geostationary hyperspectral infrared sounder observations: Progress, challenges, and future perspectives. *Bulletin of the American Meteorological Society*, *103*(12), E2733–E2755. https://doi.org/10.1175/bams-d-21-0328.1

Li, J., Santek, D., Li, Z., Lim, A., Di, D., Min, M., et al. (2025). Tracking atmospheric motions for obtaining wind estimates using satellite observations – From 2D to 3D. *Bulletin of the American Meteorological Society*, *106*(2), E344–E363. https://doi.org/10.1175/BAMS-D-24-0027.1

Li, J., Zhang, Y., Di, D., Ma, Z., Li, Z., Schmit, T. J., & Menzel, W. P. (2022). The influence of sub-footprint cloudiness on three-dimensional horizontal wind from geostationary hyperspectral infrared sounder observations. *Geophysical Research Letters*, *49*(11), e2022GL098460. https://doi.org/10.1029/2022gl098460

Li, J., Zheng, J., Li, B., Min, M., Liu, Y., Liu, C. Y., et al. (2024). Quantitative applications of weather satellite data for nowcasting: Progress and challenges. *Journal of Meteorological Research*, *38*(3), 399–413. https://doi.org/10.1007/s13351-024-3138-6

Li, Z., Schmit, T. J., Li, J., Li, J., & Heidinger, A. (2023). Studies regarding the ensquared energy of a geostationary hyperspectral infrared sounder. *IEEE Transactions on Geoscience and Remote Sensing*, *61*, 1–9. https://doi.org/10.1109/TGRS.2023.3271931

Lindsey, D. T., Heidinger, A. K., Sullivan, P. C., McCorkel, J., Schmit, T. J., Tomlinson, M., et al. (2024). GeoXO: NOAA's future geostationary satellite system. *Bulletin of the American Meteorological Society*, *105*(3), E660–E679. https://doi.org/10.1175/bams-d-23-0048.1

Ma, Z., Li, J., Han, W., Li, Z., Zeng, Q., Menzel, W. P., et al. (2021). Four-dimensional wind fields from geostationary hyperspectral infrared sounder radiance measurements with high temporal resolution. *Geophysical Research Letters*, *48*(14), e2021GL093794. https://doi.org/10.1029/2021gl093794

Ma, Z., Li, Z., Li, J., Schmit, T. J., Cucurull, L., Atlas, R., & Sun, B. (2021). Enhance low level temperature and moisture profiles through combining NUCAPS, ABI observations, and RTMA analysis. *Earth and Space Science*, *8*(6), e2020EA001402. https://doi.org/10.1029/2020ea001402



19448007, 2025, 12, Downloaded from https://agupubs.onlinelibrary.wiley.com/doi/10.1029/2025GL115548 by Ewha Womans University Library, Wiley Online Library on [07/12/2025]. See the Terms and Conditions (https://onlinelibrary.wiley.com/terms-and-conditions) on Wiley Online Library for rules of use; OA articles are governed by the applicable Creative Commons License

Meng, D., Tan, Z. M., Li, J., Ma, Z., & Chen, Y. (2024). Added value of three-dimensional horizontal winds from Geostationary Interferometric Infrared Sounder for typhoon forecast in a regional NWP model. *Journal of Geophysical Research: Atmospheres*, *129*(6), e2024JD040736. https://doi.org/10.1029/2024jd040736

Menzel, W. P., Schmit, T. J., Zhang, P., & Li, J. (2018). Satellite-based atmospheric infrared sounder development and applications. *Bulletin of the American Meteorological Society*, *99*(3), 583–603. https://doi.org/10.1175/bams-d-16-0293.1

Saunders, R., Hocking, J., Turner, E., Rayer, P., Rundle, D., Brunel, P., et al. (2018). An update on the RTTOV fast radiative transfer model (currently at version 12). *Geoscientific Model Development*, *11*(7), 2717–2737. https://doi.org/10.5194/gmd-11-2717-2018

Wang, H., Han, W., Li, J., Chen, H., & Yin, R. Y. (2025). Impact of assimilation of FY-4A GIIRS three-dimensional horizontal winds observations on typhoon forecasts. *Advances in Atmospheric Sciences*, *42*(3), 467–485. https://doi.org/10.1007/s00376-024-4051-8

Wedi, N. P., Polichtchouk, I., Dueben, P., Anantharaj, V. G., Bauer, P., Boussetta, S., et al. (2020). A baseline for global weather and climate simulations at 1 km resolution. *Journal of Advances in Modeling Earth Systems*, *12*(11), e2020MS002192. https://doi.org/10.1029/2020MS002192

Yin, R., Han, W., Gao, Z., & Li, J. (2021). Impact of high temporal resolution FY-4A Geostationary Interferometric Infrared Sounder (GIIRS) radiance measurements on Typhoon forecasts: Maria (2018) case with GRAPES global 4D-Var assimilation system. *Geophysical Research Letters*, *48*(15), e2021GL093672. https://doi.org/10.1029/2021gl093672

Zhou, R., Di, D., Li, J., & Li, Z. (2025). Enhanced moisture retrieval near boundary layer from satellite sounder data through atmospheric-surface radiance separation. *Geophysical Research Letters*, *52*(5), e2024GL113404. https://doi.org/10.1029/2024GL113404



19448007, 2025, 12, Downloaded from https://agupubs.onlinelibrary.wiley.com/doi/10.1029/2025GL115548 by Ewha Womans University Library, Wiley Online Library on [07/12/2025]. See the Terms and Conditions (https://onlinelibrary.wiley.com/terms-and-conditions) on Wiley Online Library for rules of use; OA articles are governed by the applicable Creative Commons License